

Ionic-heterogeneity-induced spiral- and scroll-wave turbulence in mathematical models of cardiac tissue

Soling Zimik¹, Rupamanjari Majumder^{2,*} and Rahul Pandit^{1†}

¹*Centre for Condensed Matter Theory,
Department of Physics, Indian Institute of Science,
Bangalore, 560012, India.*

²*Laboratory for Fluid Physics,
Pattern Formation and Biocomplexity,
Max Planck Institute for Dynamics and Self-Organization,
37077 Göttingen, Germany*

(Dated: February 21, 2022)

Spatial variations in the electrical properties of cardiac tissue can occur because of cardiac diseases. We introduce such gradients into mathematical models for cardiac tissue and then study, by extensive numerical simulations, their effects on reentrant electrical waves and their stability in both two and three dimensions. We explain the mechanism of spiral- and scroll-wave instability, which entails anisotropic thinning in the wavelength of the waves because of anisotropic variation in its electrical properties.

PACS numbers: 87.19.Hh, 89.75.-k

Nonlinear waves in the form of spirals occur in many excitable media, examples of which include Belousov-Zhabotinsky-type systems [1], calcium-ion waves in *Xenopus* oocytes [2], the aggregation of *Dictyostelium discoideum* by cyclic-AMP signaling [3], the oxidation of carbon monoxide on a platinum surface [4], and, most important of all, cardiac tissue [5]. Understanding the development of such spiral waves and their spatiotemporal evolution is an important challenge in the study of extended dynamical systems, in general, and especially in cardiac tissue, where these waves are associated with abnormal rhythm disorders, which are also called arrhythmias. Cardiac tissue can support many patterns of nonlinear waves of electrical activation, like traveling waves, target waves, and spiral and scroll waves [6]. The occurrence of spiral- and scroll-wave turbulence of electrical activation in cardiac tissue has been implicated in the precipitation of life-threatening cardiac arrhythmias like ventricular tachycardia (VT) and ventricular fibrillation (VF), which destroy the regular rhythm of a mammalian heart and render it incapable of pumping blood. These arrhythmias are the leading cause of death in the industrialized world [7–11].

Biologically, VF can arise because of many complex mechanisms. Some of these are associated with the development of instability-induced spiral- or scroll-wave turbulence [12]. One such instability-inducing factor is ionic heterogeneity [13, 14], which arises from variations in the electrophysiological properties of cardiac cells (myocytes), like the morphology and duration of their action-potentials (*APs*) [15–18]. Such variations may appear in cardiac tissue because of electrical remodeling [19–

21], induced by alterations in ion-channel expression and activity, which arise, in turn, from diseases [22] like ischemia [23, 24], some forms of cardiomyopathy [25], and the long-QT syndrome [26]. To a certain extent, some heterogeneity is normal in healthy hearts; and it has an underlying physiological purpose [16, 27–31]; but, if the degree of heterogeneity is more than is physiologically normal, it can be arrhythmogenic [20, 24, 32]. It is important, therefore, to explore ionic-heterogeneity-induced spiral- or scroll-wave turbulence in mathematical models of cardiac tissue, which allow us to control this heterogeneity precisely, in order to be able to identify the nonlinear-wave instability that leads to such turbulence. We initiate such a study by examining the effects of this type of heterogeneity in three cardiac-tissue models, which are, in order of increasing complexity and biological realism, (a) the two-variable Aliev-Panfilov model [33], (b) the ionically realistic O’Hara-Rudy (ORd) model [34] in two dimensions (2D), and (c) the ORd model in an anatomically realistic simulation domain. In each one of these models, we control parameters (see below) in such a way that the ion-channel properties change anisotropically in our simulation domains, thereby inducing an anisotropic spatial variation in the local action potential duration *APD*. We show that this variation in the *APD* leads, in all these models, to an anisotropic reduction of the wavelength of the spiral or scroll waves; and this anisotropic reduction of the wavelength paves the way for an instability that precipitates turbulence, the mathematical analog of VF, in these models.

The Aliev-Panfilov model provides a simplified description of an excitable cardiac cell [33]. It comprises a set of coupled ordinary differential equations (ODEs), for the normalized representations of the transmembrane potential V and the generalized conductance r of the slow,

* rupamanjari.majumder@ds.mpg.de

† rahul@iisc.ac.in; also at Jawaharlal Nehru Centre for Advanced Scientific Research, Bangalore, Karnataka, India

I_{Na}	fast inward Na^+ current
I_{to}	transient outward K^+ current
I_{CaL}	L-type Ca^{2+} current
I_{Kr}	rapid delayed rectifier K^+ current
I_{Ks}	slow delayed rectifier K^+ current
I_{K1}	inward rectifier K^+ current
I_{NaCa}	Na^+/Ca^{2+} exchange current
I_{NaK}	Na^+/K^+ ATPase current
I_{Nab}	Na^+ background current
I_{Cab}	Ca^{2+} background current
I_{pCa}	sarcolemmal Ca^{2+} pump current
I_{Kb}	K^+ background current
I_{CaNa}	Na^+ current through the L-type Ca^{2+} channel
I_{CaK}	K^+ current through the L-type Ca^{2+} channel

TABLE I. The various ionic currents incorporated in the ORd model are tabulated above. The symbols used for the currents follow Ref. [34].

repolarizing current:

$$\frac{dV}{dt} = -kV(V - a)(V - 1) - Vr; \quad (1)$$

$$\frac{dr}{dt} = [\epsilon + \frac{\mu_1 r}{\mu_2 + V}] [-r - kV(V - b - 1)]; \quad (2)$$

fast processes are governed by the first term in Eq.(1), whereas, the slow, recovery phase of the AP is determined by the function $\epsilon + \frac{\mu_1 r}{\mu_2 + V}$ in Eq.(2). The parameter a represents the threshold of activation and k controls the magnitude of the transmembrane current. We use the standard values for all parameters [33], except for the parameter k . We write $k = g \times k_o$, where g is a multiplication factor and k_o is the control value of k . In 2D simulations we introduce a spatial gradient (a linear variation) in the value of k along the vertical direction of the domain. To mimic the electrophysiology of a human ventricular cell, we perform similar studies using a slightly modified version of the ionically-realistic O'Hara-Rudy model (ORd) [34, 35]. Here, the transmembrane potential V is governed by the ODE

$$\frac{dV}{dt} = -\frac{I_{ion}}{C_m}, \quad I_{ion} = \sum_x I_x, \quad (3)$$

where I_x , the membrane ionic current, for a generic ion channel x , of a cardiac cell, is

$$I_x = G_x f_1(p_{act}) f_2(p_{inact}) (V_m - E_x), \quad (4)$$

where $C_m = 1 \mu F$ is the membrane capacitance, $f_1(p_{act})$ and $f_2(p_{inact})$ are, respectively, functions of probabilities of activation (p_{act}) and inactivation (p_{inact}) of the ion channel x , and E_x is its Nernst potential. We give a list of all the ionic currents in the ORd model in Table I. We write $G_x = g \times G_{xo}$, where G_{xo} is the original value of the maximal conductance of the ion channel x in the

ORd model, and g is a multiplication factor. We model gradients in G_x as follows:

$$G_x(y) = [g_{min} + \frac{y(g_{max} - g_{min})}{L}] G_{xo}, 0 \leq y \leq L; \quad (5)$$

here, L is the length of the side of the square simulation domain, and g_{max} and g_{min} are, respectively, the maximal and minimal values of g ; we can impose gradients in k in the Aliev-Panfilov model in the same manner. For simplicity, we induce the gradient along one spatial direction only: the vertical axis in 2D; and the apico-basal (apex-to-base) direction in 3D. The spatiotemporal evolution of V in both models is governed by the following reaction-diffusion equation:

$$\frac{\partial V}{\partial t} + I = \nabla \cdot (\mathcal{D} \nabla V), \quad (6)$$

where \mathcal{D} is the diffusion tensor, and $I = \frac{I_{ion}}{C_m}$ and $kV(V - a)(V - 1) + Vr$ for ORd and Aliev-Panfilov models, respectively. For the numerical implementation of the diffusion term in Eq. (6), we follow Refs. [35, 36]. We construct our anatomically realistic simulation domain with processed human-ventricular data, obtained by using Diffusion Tensor Magnetic Resonance Imaging (DTMRI) [37].

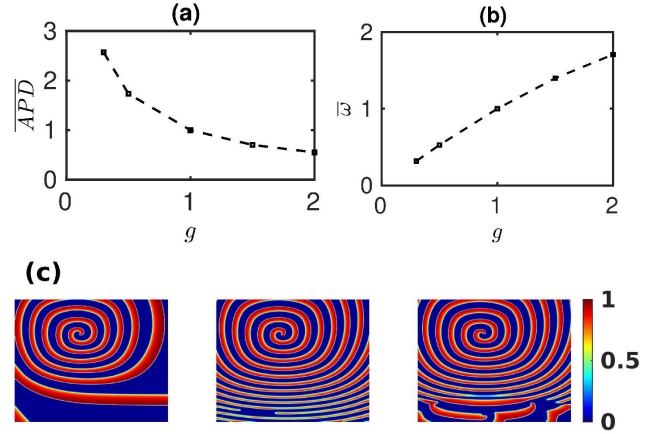


FIG. 1. (Color online) Variation of (a) \overline{APD} and (b) \bar{w} (see text) with k . $\overline{APD} = APD/APD_o$; here, APD_o is the control value of APD at $g = 1$ (so $\overline{APD} = 1$ at $g = 1$); we also use other combinations of (\overline{APD}, g) in our numerical simulations. We find that \overline{APD} decreases with increasing k ; however, \bar{w} increases with increasing k . (c) Pseudocolor plots of V , at three representative times (time increases from left to right), illustrating the precipitation of the spiral-wave instability in the Aliev-Panfilov model with a linear gradient in k ; the video S1 in the Supplemental Material [38] shows the complete spatiotemporal evolution of this instability.

In Fig. 1(a) we show the variation, with the parameter g , of $\overline{APD} = APD/APD_o$, where APD_o is the control APD value for $g = 1$. We find that \overline{APD} decreases with increasing g . Changes in the APD at the single-cell level

influence electrical-wave dynamics at the tissue level. In particular, such changes affect the rotation frequency ω of reentrant activity (spiral waves). If θ and λ denote, respectively, the conduction velocity and wavelength of a plane electrical wave in tissue, then $\omega \simeq \frac{\theta}{\lambda}$, $\lambda \simeq \theta \times APD$. Therefore, if we neglect curvature effects [39], the spiral-wave frequency

$$\omega \simeq \frac{1}{APD}. \quad (7)$$

We find, in agreement with this simple, analytical estimate, that ω decreases as the APD increases. We show this in Fig. 1(b) by plotting $\bar{\omega} = \omega/\omega_0$ versus g ; here, ω_0 is the frequency for $g = 1$ [40].

Similarly, in the ionically realistic ORd model, changes in the ion-channel conductances G_x alter the APD of the cell and, therefore, the spiral-wave frequency ω . In Figs. 2 (a1) and (a2) we present a family of plots to illustrate the variation in \overline{APD} with changes in G_x . We find that \overline{APD} decreases with an increase in g for most currents (I_{Kr} , I_{Ks} , I_{K1} , I_{Na} and I_{NaK}); but it increases for some other currents (I_{Ca} , I_{NaCa} and I_{to}). The rate of change of \overline{APD} is most significant when we change G_{Kr} ; by contrast, it is most insensitive to changes in G_{Na} and G_{to} . In Figs. 2 (b1) and (b2) we show the variation of $\bar{\omega}$ with g for different ion channels x . We find that changes in G_x , which increase APD , decrease ω and vice versa; this follows from Eq. (2). The sensitivity of ω , with respect to changes in G_x , is most for $G_x = G_{Kr}$ and least for $G_x = G_{to}$: $\bar{\omega}$ increases by $\Delta\bar{\omega} \simeq 1.23$, as g goes from 0.2 to 5; for G_{to} , the same variation in g decreases the value of $\bar{\omega}$ by $\Delta\bar{\omega} \simeq 0.04$.

We now investigate the effects, on spiral-wave dynamics, of spatial gradients in k , in the 2D Aliev-Panfilov model, and in G_x , in the 2D ORd model. A linear gradient in k , in the Aliev-Panfilov model, induces a gradient in $\bar{\omega}$ (see Fig. 1(b)); and such a spatial gradient in $\bar{\omega}$ induces a spiral-wave instability in the low- $\bar{\omega}$ region. In Fig. 1(c) we demonstrate how a gradient in k ($g_{max} = 1.5$ and $g_{min} = 0.5$) leads to the precipitation of this instability (also see video S1 of the Supplemental Material [38]).

Similarly, for each current listed in Table I for the ORd model, we find wave breaks in a medium with a gradient in G_x . We illustrate, in Fig. 3, such wave breaks in our 2D simulation domain, with a gradient (∇G_x) in any G_x , for 3 representative currents; we select I_{Kr} , because it has the maximal impact on the single-cell APD , and also on ω in tissue simulations; and we choose I_{K1} and I_{NaCa} , because they have moderate and contrary effects on APD and ω (Figs. 2). Our results indicate that gradient-induced wave breaks are generic, insofar as they occur in both the simple two-variable (Aliev-Panfilov) and the ionically realistic (ORd) models of cardiac tissue. In Figs. 3 (d-f), we present power spectra of the time series of V , recorded from a representative point of the simulation domain; these spectra show broad-band backgrounds, which are signatures of chaos, for the gradients ∇G_{Kr} and ∇G_{K1} ; however, the gradient ∇G_{NaCa}

induces wave breaks while preserving the periodicity of the resultant, reentrant electrical activity, at least at the points from which we have recorded V .

The instability in spiral waves occurs because spatial gradients in k (Aliev-Panfilov) or in G_x (ORd) induce spatial variations in both \overline{APD} and $\bar{\omega}$: In our simulation domain, the local value of $\bar{\omega}$ (\overline{APD}) decreases (increases) from the top to the bottom. In the presence of a single spiral wave (left panel of Fig. 4), the domain is paced, in effect, at the frequency ω of the spiral, i.e., with a fixed time period $T = 1/\omega = APD + DI$, where DI is the diastolic interval (the time between the repolarization of one AP and the initiation of the next AP). Thus, the bottom region, with a long APD , has a short DI and vice versa. The restitution of the conduction velocity θ implies that a small DI leads to a low value of θ and vice versa [41] (see Fig. S1 in the Supplemental Material [38]). To compensate for this reduction of θ , the spiral wave must reduce its wavelength λ , in the bottom, large- APD (small- DI) region, so that its rotation frequency $\omega \simeq \frac{\theta}{\lambda}$ remains unchanged, as shown in Fig. 4 (also see video S2 in the Supplemental Material [38]), where the thinning of the spiral arms is indicated by the variation of λ along the spiral arm ($\lambda_2 > \lambda_1$, in the pseudocolor plot of V_m in the top-left panel $t = 1.46$ s). Clearly, this thinning is anisotropic, because of the uni-directional variation in k or G_x ; this anisotropy creates functional heterogeneity in wave propagation, which leads in turn to the spiral-wave instability we have discussed above (Fig. 4).

In the ORd model, we find that gradients in G_{Kr} easily induce instabilities of the spiral for small values of $\Delta g \equiv g_{max} - g_{min} \simeq 0.5$; by contrast, in a medium with gradients in G_{to} , the spiral remains stable for values of Δg as large as 4.8. This implies that the stability of the spiral depends on the magnitude of the gradient in ω that is induced in the medium.

In Fig. 5 (also see video S3 in the Supplemental Material [38]), we extend our study to illustrate the onset of scroll-wave instabilities in a 3D, anatomically realistic human-ventricular domain, in the presence of spatial gradients in G_{Kr} . In mammalian hearts, the APD is typically lower in the apical region as compared to that in the basal region [16]. Therefore, we use values of the APD that increase from the apex to the base (and, hence, ω decreases from the apex to base). With $g_{max}(G_{Kr}) = 6$ and $\Delta g = 4$, we observe breakup in a scroll wave that is otherwise stable in the absence of this spatial gradient. We note that the mechanism for the onset of such scroll-wave instabilities is the same as in 2D, and it relies on the gradient-induced anisotropic thinning of the scroll wavelength.

We have shown that gradients in parameters that affect the APD of the constituent cells induce spatial gradients in the local value of ω . This gradient in the value of ω leads to an anisotropic reduction in the wavelength of the waves, because of the conduction-velocity restitution property of the tissue, and it paves the way for spiral- and scroll-wave instability in the domain. This gradient-

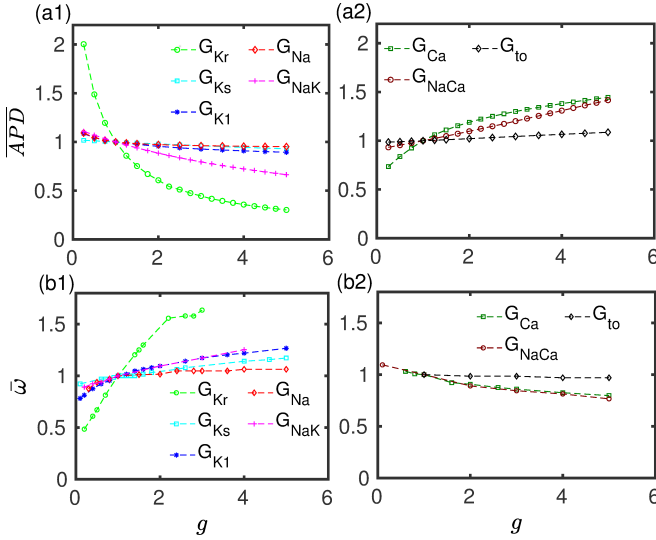


FIG. 2. (Color online) Plots of \overline{APD} and $\bar{\omega}$ versus g ; here, $\overline{APD} = APD/APD_o$ and $\bar{\omega} = \omega/\omega_0$, where $APD_o = 250$ ms, and $\omega_0 = 4.38$ Hz are, respectively, the control values of APD and ω ; (a1) and (a2) show, respectively, that \overline{APD} decreases with the conductances G_x , for the currents I_{Kr} , I_{Ks} , I_{K1} , I_{Na} and I_{NaK} ; however, it increases with increasing G_x , for the currents I_{CaL} , I_{NaCa} and I_{to} ; (b1) and (b2) show that the variation of $\bar{\omega}$, with the various channel conductances, is consistent with Eq. (2).

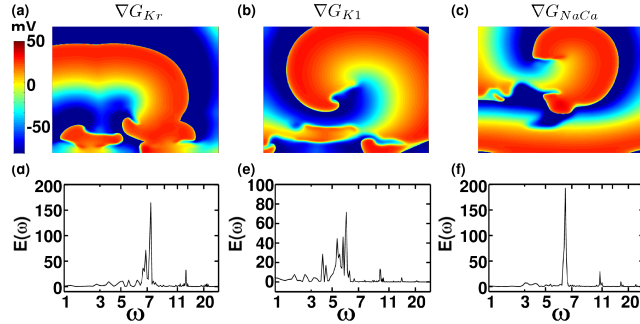


FIG. 3. (Color Online) Pseudocolor plots of the transmembrane potential V_m illustrating spiral-wave instabilities from our numerical simulations of the 2D ORd model for human ventricular tissue, with spatial gradients in (a) G_{Kr} , (b) G_{K1} , and (c) G_{NaCa} (because G_{NaCa} decreases with g (Fig. 2), the gradient in G_{NaCa} must be chosen to be the negative of that in Eq. (5)); in (a)-(c) the local value of ω decreases from the top of the simulation domain to its bottom. Power spectra of the time series of V_m , from representative points in our simulation domain, are shown for gradients in (d) G_{Kr} , (e) G_{K1} , and (f) G_{NaCa} ; the spectra in (d) and (e) are consistent with the onset of spiral-wave turbulence; the power spectrum in (f) shows the continuation of periodic electrical activity, in spite of wave breaks.

induced instability is a generic phenomenon because we obtain this instability in the simple Aliev-Panfilov and the detailed ORd model for cardiac tissue. Such an instability should be observable in any excitable medium that

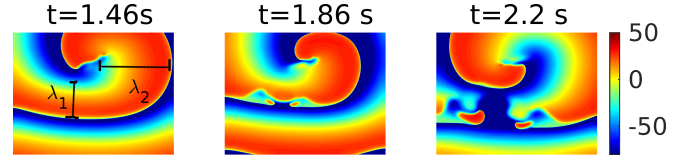


FIG. 4. (Color Online) Pseudocolor plots of V_m illustrating the development of a spiral-wave instability, with the passage of time t , in the 2D ORd model, with a spatial gradient in G_{NaCa} . The left frame shows the thinning of the spiral arm (λ varies along the spiral arm, and $\lambda_2 > \lambda_1$) indicated just before the spiral wave breaks (see the middle and the right frames).

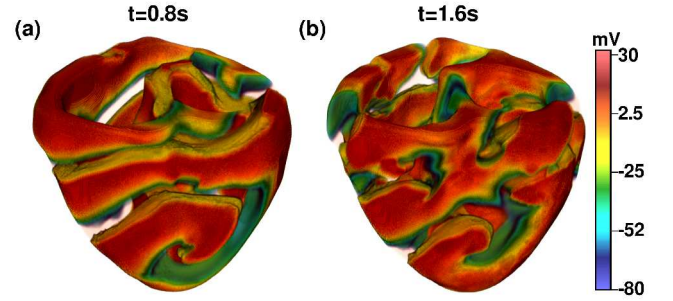


FIG. 5. (Color Online) Scroll-wave instabilities in our anatomically realistic human-ventricular domain, in the presence of an apico-basal gradient in G_{Kr} .

has the conduction-velocity-restitution property. We find that the spiral or scroll waves always break up in the low- ω region. This finding is in line with that of the experimental study by Campbell, *et al.*, [15] who observe spiral-wave break-up in regions with a large APD in neonatal-rat-ventricular-myocyte cell culture. We find that the stability of the spiral is determined by the magnitude of the gradient in ω ; the larger the magnitude of the gradient in the local value of ω , the more likely is the break up of the spiral or scroll wave. By using the ORd model, we find that ω varies most when we change G_{Kr} (as compared to other ion-channel conductances) and, therefore, spiral waves are most unstable in the presence of a gradient of G_{Kr} . By contrast, we find that ω varies most gradually with G_{to} , and hence the spiral wave is most stable in the presence of a gradient in G_{to} (as compared to gradients in other conductances).

Earlier studies have investigated the effects of ionic-heterogeneity on spiral-wave dynamics. The existence of regional ionic heterogeneities have been found to initiate spiral waves [42], attract spiral waves to the heterogeneity [43], and destabilize spiral waves [44]. The presence of APD gradients in cardiac tissue has been shown to drive spirals towards large- APD (low ω) regions [45]. A study by Zimik, *et al.*, [35] finds that spatial gradients in ω , induced by gradients in the density of fibroblasts, can precipitate a spiral-wave instability. However, none of these studies provides a clear understanding of the mechanisms

underlying the onset of spiral- and scroll-wave instabilities, from a fundamental standpoint. Moreover, none of these studies has carried out a detailed calculation of the pristine effects of each individual major ionic currents, present in a myocyte, on the spiral-wave frequency; nor have they investigated, in a controlled manner, how gradients in ion-channel conductances lead to spiral- or scroll-wave instabilities. Our work makes up for these lacunae and leads to specific predictions that should be tested experimentally.

ACKNOWLEDGMENTS

We thank the Department of Science and Technology (DST), India, and the Council for Scientific and Industrial Research (CSIR), India, for financial support, and Supercomputer Education and Research Centre (SERC, IISc) for computational resources.

-
- [1] A. Zaikin and A. Zhabotinsky, *Nature* **225**, 535 (1970).
 - [2] D. E. Clapham, *Cell* **80**, 259 (1995).
 - [3] J. J. Tyson and J. Murray, *Development* **106**, 421 (1989).
 - [4] R. Imbihl and G. Ertl, *Chemical Reviews* **95**, 697 (1995).
 - [5] J. M. Davidenko, A. V. Pertsov, R. Salomonsz, W. Baxter, and J. Jalife, *Nature* **355**, 349 (1992).
 - [6] J. J. Tyson and J. P. Keener, *Physica D: Nonlinear Phenomena* **32**, 327 (1988).
 - [7] P. Bayly, B. KenKnight, J. Rogers, E. Johnson, R. Ideker, and W. Smith, *Chaos: An Interdisciplinary Journal of Nonlinear Science* **8**, 103 (1998).
 - [8] F. X. Witkowski, L. J. Leon, P. A. Penkoske, W. R. Giles, M. L. Spano, W. L. Ditto, and A. T. Winfree, *Nature* **392**, 78 (1998).
 - [9] G. P. Walcott, G. N. Kay, V. J. Plumb, W. M. Smith, J. M. Rogers, A. E. Epstein, and R. E. Ideker, *Journal of the American College of Cardiology* **39**, 109 (2002).
 - [10] I. R. Efimov, V. Sidorov, Y. Cheng, and B. Wollenzier, *Journal of cardiovascular electrophysiology* **10**, 1452 (1999).
 - [11] J. De Bakker, F. Van Capelle, M. Janse, A. Wilde, R. Coronel, A. Becker, K. Dingemans, N. Van Hemel, and R. Hauer, *Circulation* **77**, 589 (1988).
 - [12] F. H. Fenton, E. M. Cherry, H. M. Hastings, and S. J. Evans, *Chaos: An Interdisciplinary Journal of Nonlinear Science* **12**, 852 (2002).
 - [13] G. K. Moe, W. C. Rheinboldt, and J. Abildskov, *American heart journal* **67**, 200 (1964).
 - [14] J. Jalife, *Annual review of physiology* **62**, 25 (2000).
 - [15] K. Campbell, C. J. Calvo, S. Mironov, T. Herron, O. Berenfeld, and J. Jalife, *The Journal of physiology* **590**, 6363 (2012).
 - [16] N. Szentadrassy, T. Banyasz, T. Biro, G. Szabo, B. I. Toth, J. Magyar, J. Lazar, A. Varro, L. Kovacs, and P. P. Nanasi, *Cardiovascular Research* **65**, 851 (2005).
 - [17] M. Stoll, M. Quentin, A. Molojavyi, V. Thämer, and U. K. Decking, *Cardiovascular research* (2007).
 - [18] D.-W. Liu and C. Antzelevitch, *Circulation research* **76**, 351 (1995).
 - [19] M. M. Elsharif, P. Shi, and E. M. Cherry, *IEEE journal of biomedical and health informatics* **19**, 1308 (2015).
 - [20] S. Nattel, A. Maguy, S. Le Bouter, and Y.-H. Yeh, *Physiological reviews* **87**, 425 (2007).
 - [21] M. J. Cutler, D. Jeyaraj, and D. S. Rosenbaum, *Trends in pharmacological sciences* **32**, 174 (2011).
 - [22] A. S. Amin, H. L. Tan, and A. A. Wilde, *Heart Rhythm* **7**, 117 (2010).
 - [23] A. H. Harken, C. H. Barlow, W. R. Harden, and B. Chance, *The American journal of cardiology* **42**, 954 (1978).
 - [24] X. Jie and N. A. Trayanova, *Heart Rhythm* **7**, 379 (2010).
 - [25] G. Sivagangabalan, H. Nazzari, O. Bignolais, A. Maguy, P. Naud, T. Farid, S. Massé, N. Gaborit, A. Varro, K. Nair, P. Backx, E. Vigmond, S. Nattel, S. Demolombe, and K. Nanthakumar, *PLoS ONE* **9**, e82179 (2014).
 - [26] P. C. Viswanathan and Y. Rudy, *Circulation* **101**, 1192 (2000).
 - [27] C. Antzelevitch, S. Sicouri, S. H. Litovsky, A. Lukas, S. C. Krishnan, J. M. Di Diego, G. A. Gintant, and D.-W. Liu, *Circ Res* **69**, 1427 (1991).
 - [28] T. Furukawa, R. J. Myerburg, N. Furukawa, A. L. Bassett, and S. Kimura, *Circulation Research* **67**, 1287 (1990).
 - [29] D. Fedida and W. Giles, *The Journal of Physiology* **442**, 191 (1991).
 - [30] S. Zicha, L. Xiao, S. Stafford, T. J. Cha, W. Han, A. Varro, and S. Nattel, *The Journal of physiology* **561**, 735 (2004).
 - [31] F. H. Samie, O. Berenfeld, J. Anumonwo, S. F. Mironov, S. Udassi, J. Beaumont, S. Taffet, A. M. Pertsov, and J. Jalife, *Circulation research* **89**, 1216 (2001).
 - [32] M. J. Janse, *Cardiovascular research* **61**, 208 (2004).
 - [33] R. R. Aliev and A. V. Panfilov, *Chaos, Solitons & Fractals* **7**, 293 (1996).
 - [34] T. O'Hara, L. Virág, A. Varró, and Y. Rudy, *PLoS Comput Biol* **7**, e1002061 (2011).
 - [35] S. Zimik and R. Pandit, *New J. Phys* **18**, 123014 (2016).
 - [36] R. Majumder, R. Pandit, and A. V. Panfilov, *JETP letters* **104**, 796 (2016).
 - [37] "Dtmri data from ex-vivo canine and human hearts, the cardiovascular research center, Johns Hopkins University."
 - [38] Supplementary Information.
 - [39] Z. Qu, F. Xie, A. Garfinkel, and J. N. Weiss, *Annals of biomedical engineering* **28**, 755 (2000).
 - [40] For the parameter a this simple relation between ω and APD is not observed, because change in a affects not only the APD but also other quantities like θ , which has effects on the value of ω .
 - [41] E. M. Cherry and F. H. Fenton, *American Journal of Physiology-Heart and Circulatory Physiology* **286**, H2332 (2004).
 - [42] A. Defauw, P. Dawyndt, and A. V. Panfilov, *Physical Review E* **88**, 062703 (2013).
 - [43] A. Defauw, N. Vandersickel, P. Dawyndt, and A. V. Panfilov, *American Journal of Physiology-Heart and Circulatory Physiology* **307**, H1456 (2014).
 - [44] A. Xu and M. R. Guevara, *Chaos: An Interdisciplinary Journal of Nonlinear Science* **8**, 157 (1998).
 - [45] K. Ten Tusscher and A. V. Panfilov, *American Journal of*

Physiology-Heart and Circulatory Physiology **284**, H542 (2003).

Supplemental Material

Electrical-wave turbulence in anisotropic cardiac tissue

Soling Zimik¹, Rupamanjari Majumder², and Rahul Pandit¹

¹Centre for Condensed Matter Theory, Department of Physics, Indian Institute of Science, Bangalore, 560012, India

²Laboratory for Fluid Physics, Pattern Formation and Biocomplexity, Max Planck Institute for Dynamics and Self-Organization, 37077 Göttingen, Germany

Video Captions:

Video S1: **Spiral-wave instability in the Aliev-Panfilov model.** Video of pseudocolor plots of transmembrane potential V showing the formation of spiral-wave instability in a medium with gradient in k : $g_{min}=0.5$ and $g_{max}=1.5$. For the video, we use 10 frames per second with each frame separated from the succeeding frame by 20ms in real time.

Video S2: **Spiral-wave instability in the ORd model.** Video pseudocolor plots of transmembrane potential V_m showing the formation of spiral-wave instability in a medium with a gradient in G_{Naca} ($g_{min}=0.2$ and $g_{max}=2$). For the video, we use 10 frames per second with each frame separated from the succeeding frame by 20ms in real time.

Video S3: **Scroll-wave instability.** Video pseudocolor plots of transmembrane potential V_m showing the formation of scroll-wave instability in an anatomically-realistic model for human ventricles. A linear gradient in G_{Kr} is applied along the apico-basal direction: $g_{min} = 2$ in the apex and $g_{max}=6$ in the base. For the video, we use 10 frames per second with each frame separated from the succeeding frame by 20ms in real time.

Figures:

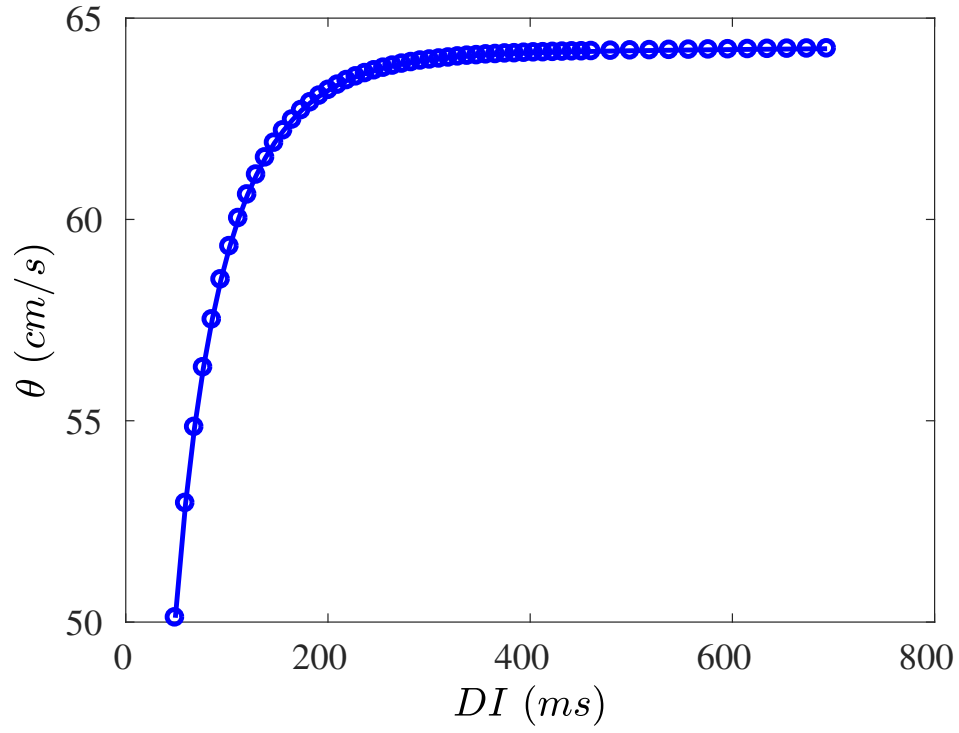


Figure showing a conduction-velocity restitution curve, generated by using the ORd model. The value of conduction velocity θ initially increases with the increase of diastolic interval DI and saturates at large values of DI .